09-05-2016

Quantification of ASL and DTI Data in the Brain of Patients with Alzheimer's Disease

GRADUATION THESIS

L.B. VAN DEN OEVER

GRADUATION COMMITTEE

PROF. DR. IR. C.H. SLUMP	CHAIRMAN COMMITTEE
J.A.H.R. CLAASSEN, MD, PHD	MEDICAL SUPERVISOR
DRS. P. VAN KATWIJK	PROCESS SUPERVISOR
D.L.K. DE JONG, MSC	EXTRA MEMBER
IR. F.F.J. SIMONIS	EXTERNAL MEMBER

Table of Contents

Chapter 1

“Quantifying ASL and DTI”

1 Problem Definition

This master thesis describes a part of a large research project that investigates a new treatment for Alzheimer's disease (AD). During this project, magnetic resonance images (MRI) of the brain were made in patients with AD. With the data from this research, we investigated the pathophysiology of AD. AD is a neurodegenerative disorder that manifests itself in memory loss, location and time mismatches, mood swings and changes in personality and behaviour. The cause of AD is largely unknown. Changes in perfusion are present in AD and thought to have an effect on the functioning of the brain. It is unknown where these perfusion changes originate, what causes them and what effect hypoperfusion has on the brain tissue itself. Although we will discuss this further in chapter 2 of this thesis, we want to investigate the effect of perfusion of brain regions on the white matter tracts in the brain. Perfusion can be measured with a magnetic resonance imaging (MRI) sequence called arterial spin labelling (ASL), while white matter integrity can be measured with diffusion tensor imaging (DTI). There are many different ways to analyse MR data. All of them have to be adapted for use in specific modalities and patient groups, so we will have to develop a processing pipeline to quantify both ASL data and DTI data.

2 Purpose

We want to automatically quantify ASL and DT data of brain regions affected by AD in patients with AD so we can investigate the effects of perfusion changes on the white matter. We expected that hypoperfusion had a negative effect on the white matter integrity.

3 Requirements

The raw image files that the Siemens Mangetom TrioTim Syngo MR machine creates are .ima files. The first requirement, therefore, was that our pipeline is able to process these files. We were given data from each different scanning sequence. We needed to sort and rename this data for easier handling.

We decided to use the FMRIB group's library of analysis tools[1–3], because these tools are known to be able to work with sequences with multiple inversion times (TI). These tools required the data to be in nifti format, so we needed a way to convert these images from .IMA to .nii.gz. It can happen that the number of image files between patients differs, since a scan can be redone if the patient moves during scanning. This meant that we could not give a limit to the number of files used.

The database that was available to us contained 50 MR datasets. Therefore, we wanted the pipeline to be automated to save time. It will also make sure there are no human-induced differences in analysis between patients, as each patient will be analysed the same way. We aimed for as little input as possible.

Both ASL and DTI are very susceptible for artefacts. We needed to correct for at least motion artefacts, eddy currents in DTI and cerebral atrophy.

For analysis, we wanted to compare regions in the brain. We selected 10 regions of interest within in the brain. Six of these regions have shown hypoperfusion in AD in previous studies, two are control regions and we used the cingulum as the white matter tract of interest and divided it in a posterior and anterior part. We separated the left and right sides of the regions so that we could detect differences and use it later as part of quality control later. With ASL, perfusion maps giving absolute flow per voxel could be created. However, between patients, absolute flow can differ significantly in values. This makes it difficult to localize hypoperfusion with only absolute values. We decided to normalize the data so we could find hypo- or hyperperfused areas between patients. The output of

the pipeline should be the normalized perfusion data of each region in both the left and right hemisphere. For the white matter analysis, we did the same for the FA and MD data as we did with the ASL data.

For our correlation analysis, we used SPSS. We had 10 regions we wanted to investigate. We wanted to analyse the right and left side separately, so that will leave us with 20 regions per modality. To be able to insert these regional values into SPSS, we wanted the output to be a Microsoft Excel file, from which the values can be easily copied into SPSS.

We also wanted to create a form of automated quality control of the data. Although we will need to check the images in the end, the registration tools are capable of producing quality control output. This output could be used to create a way to do quality control.

Table 1 shows an overview of all the requirements that we had at the beginning of our development.

Table 1: Summary of the processing pipeline its requirements.

Requirements of Pipeline
Automated
Process multiple TI data
Convert DICOM files
Organize MR files
Correct for misalignment or motion artefacts
Register data to standard space
Create calibrated map of perfusion data
Create FA and MD maps
Calculate FA, MD and perfusion values per region
Allow for easy extraction of values to SPSS
Create forms of quality control

4 Design

We started with the organisation of our data. The MR scans of one patient provide us with a total of 2000 image files, divided in ASL, T1, DTI and M0 images. There are patient IDs, study names and dates in the names of these files. For anonymous use of these files, we needed to rename them and convert them for further use. Rorden's DCM2NII tool[4] let us convert files from image to nifty format. It also allowed us to anonymize the data and rename it. The files that we get as output now consist only of the sequence used and a number. In the case of the ASL sequence, the images came in batches of three, the first being the tagged image, the second the control image and the third the difference image for each different bolus duration. The DT images are rotating images which we will not have to sort further. We also kept the T1 weighted image for creating a brain mask later on. The MRI machine will correct the T1 if the T1 is disoriented, meaning the anterior side of the face is not orientated upwards in the x-y view. Figure 1 shows a disoriented T1 versus a reoriented T1 weighted image. We had to select the correct image.

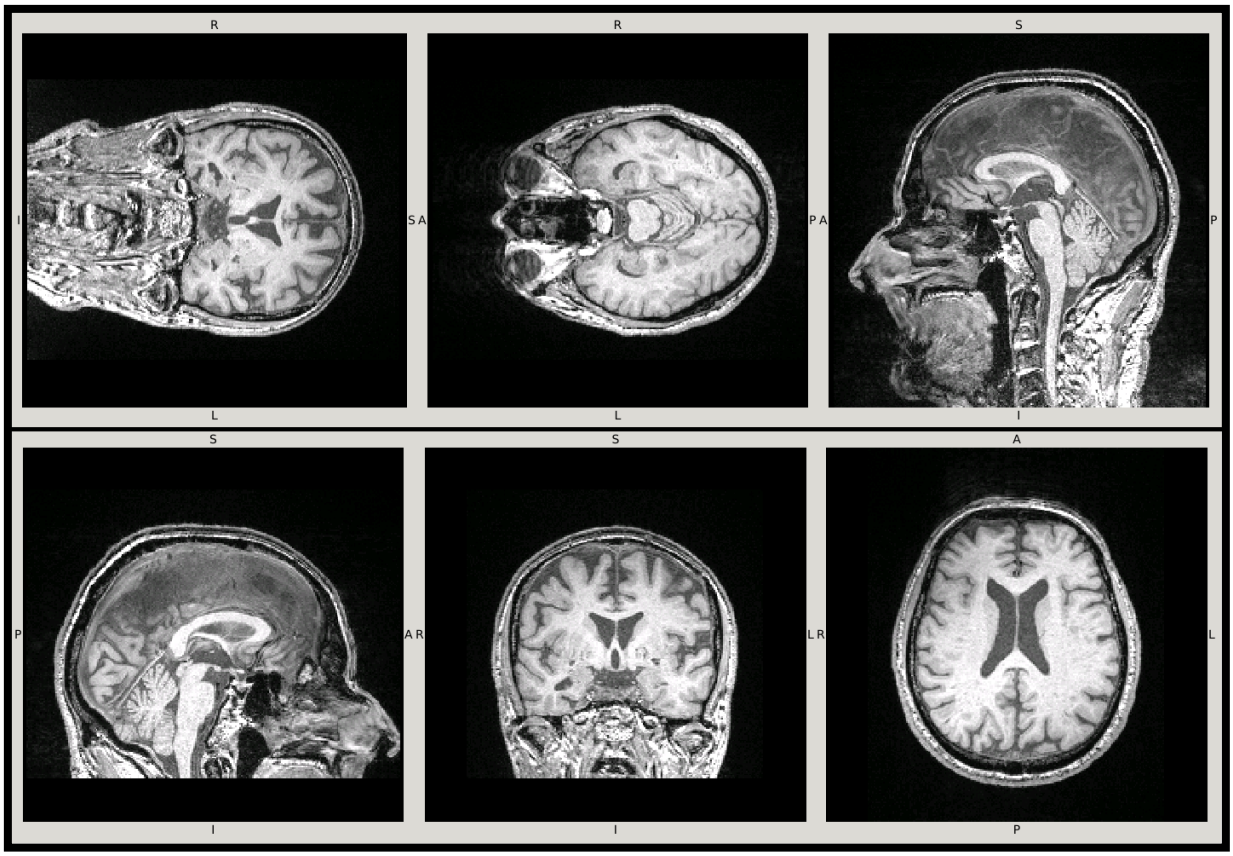

Figure 1: Example of reorientation done by the MR software. The upper three images show the T1 weighted image as acquired by the MR and the lower three show the reorientation that is done by the software of the MR machines.

4.1 ASL Processing

For our research, we need perfusion maps of the brain of all our patients. This means we have to collect the ASL datasets, which are tagged and untagged images, and subtract them from each other. This will be the input for the OXFORD_ASL tool, which can calculate the perfusion values with the help of an M0 image. The perfusion maps will then be divided into specific regions to extract the average perfusion values per region.

The pipeline moves all the files to separate folders per sequence and renames them so that the pipeline can easily recall them when needed. We used a personal identification number (PIN) for each patient that links our data to specific patients for anonymities sake. We gave the PIN as input right at the start so that we did not have to give any input when the program is running. The study which the data was acquired from has three measurements, the first at the start of the study, the baseline or T0, and two follow-up measurement, one after half a year, the T1, and one a year after the T1, T2. The names of the image files now consisted of the PIN, the timepoint, the sequence and an ascending number per file. For the ASL files, it is important to keep the right order, since the files are linked to each other as discussed earlier.

The first quality control check was built in after this moment. The normal number of TIs for our data is 10. If this number differs from the number of files, the pipeline gives this as a warning at the end of the pipeline. This usually meant that we needed to check the files and see if the registration was correct. We use one of the images with a longer TI for registration, because the contrast is usually better. If the number of TIs more than 10, it is possible that the patient moved and the scan had to be redone. The previous scans were not discarded so we got a longer series of perfusion scans. If we

use the same image for registration, the image is probably of lesser contrast, because it is an image with shorter TI.

To filter the noise outside of the brain region and to remove the skull, we needed to extract the brain from our images. We used the brain extraction tool (BET) that is supplied by the FSL[5]. We used this tool on the ASL data, but this did not give the desired result, because of the low resolution of the data and no discernible skull. This caused large areas in the brain to be filtered out. We solved this problem by using the OXFORD_ASL tool. This toolbox uses a T1 image where BET has been used on as a mask to filter out the skull and noise outside the brain. Therefore, the pipeline used BET on the T1 so this can be used later.

The next step was also for the sake of quality control. We created 4D images of the tagged, untagged and difference files to check if any of the images are different from the others. This could be in misregistration, artefacts or intensity shifts. These files can be monitored if something goes wrong.

The MCFLIRT tool was then used to realign the slices[6]. We made a list of the tagged and untagged files and used this as an input for MCFLIRT. MCFLIRT used a reference timepoint, preferably the one with the best contrasts, and tries to register every other image to this timepoint. We chose timepoint 12, which is a high contrast tagged file, for our reference slice, since a high contrast file will improve the performance of MCFLIRT. Timepoint twelve is one of the images with a high TI. This means that more tissue is tagged in the image than in images with a lower TI. This results in more contrast in the image. We let MCFLIRT output a number of plots and statistics from which we created estimated rotation and translation per timepoint in relation to the slice we used as reference. This can be used as a quality control. If images rotate or translate much, it is usually an indication that the image quality is bad or that something went wrong.

To be able to use an atlas for our region selection, all data had to be in the same coordinate space. The atlases we used are the Harvard-Oxford[7] cortical and subcortical atlas and the JHU white-matter tractography atlas[8,9]. These atlases are in the MNI standard coordinate space. ASL data has a very low resolution. Since most registration software works by using segmentation maps, this makes registration with low resolution images very difficult. We had to develop a different approach. First, we attempted to register the ASL directly to the standard space. This caused misregistration or misorientations. The next attempt was to register the T1 to the ASL data. This also caused a lot of misregistrations because of the low resolution of the ASL data. Therefore, one of the ASL images is registered to our T1 data with the FMRIB Linear Image Registration (FLIRT) tool[6,10] and the transformation matrix is extracted. Then, we registered our T1 to the MNI standard brain, which is in the MNI standard coordinate space. We could use the transformation matrices acquired this way to transform the ASL data to standard space. By first transforming the ASL to the T1 and then to the MNI standard space, we hoped to improve the registration. This method prevented a larger transformation by registering the ASL to the standard brain in one registration. The ASL-to-T1 registration is a smaller transformation step and less susceptible to errors.

To create the difference images, the pipeline subtracted the tagged and untagged files by using the ASL_FILE tool. This tool allows manipulation of the ASL files. We needed to enter the number of different TIs we have, which was done automatically, the order in which the tagged and untagged files were, and that we wanted the difference between the two as output.

To convert the voxel values of the difference image to a meaningful perfusion value, we needed a calibration image. This calibration was done during one of the MR sequences and calculates the magnetization of arterial blood in each voxel. This M0 image was registered to the standard space

with FLIRT and the M0 values of each voxel have to be calculated. This is done by using the following equation:

$$x_{new} = \frac{x_{old}}{1 - e^{-\frac{TR}{T1_{gm}}}} \qquad (1)$$

Where x_{new} is the value of each voxel for the calibration image, x_{old} is the value of each voxel in the acquired M0 image, TR the repetition time used and $T1_{gm}$ the T1 relaxation time of grey matter.

With the OXFORD_ASL tool, the difference images could be processed into a single perfusion image based on Bayesian inference principles[11,12]. The OXFORD_ASL tool also compensated for artefacts that the data may contain and uses partial volume correction to correct for the different tissue types. A number of input values were required by this tool: The difference images, the inversion times, the bolus length and arrival time, the tissue and blood T1 values, the standard brain and the brain mask, the M0 calibrated image and the repetition time of the calibration data. Output of this tool included the calibrated single perfusion image, arterial cerebral blood volume images and an arrival time image.

4.2 DTI Processing

The DTI processing started with correcting any eddy currents that may have happened during image acquisition. The EDDY_CORRECT tool of the FSL was used to do this[13]. It also corrected simple head motion artefacts that occur by registration to a reference volume.

The next step was to filter the noise outside of the brain. This was done with the BET tool as used in the ASL processing. We had to adjust the threshold to 0.2 for use in the DTI data.

To fit a diffusion tensor vector to each voxel, the pipeline used the DTIFIT tool. This tool required the diffusion weighted data, the brain mask, the gradient directions and the b values. This tool gave the three eigenvectors, eigenvalues, the mean diffusivity and the fractional anisotropy as output. We calculated the MD by averaging the 2nd and 3rd eigenvalue.

4.3 Region Selection and Data Acquisition

We extracted the regions we needed for our research and separated the left and right part. These regions were used as masks to select only the perfusion, FA and MD values of these regions using the FSLMATHS tool, which allowed mathematic manipulation of images. We used the FSLSTATS tool to calculate the mean value of the voxels excluding the voxels with a value of zero. The values that FSLSTATS calculated were saved in a .csv file for easy extraction to SPSS.

5 Testing

The pipeline created a number of folders. In the folders DTI and FirstAnalysis, the results of the analyses can be found. In the subfolders called regions in the DTI and FirstAnalysis folders are two .csv files. These files contain the absolute perfusion and FA and MD values and one contains the ratios between the regions. In the subfolder struct_space in the FirstAnalysis folder, the calibrated perfusion image can be found. Viewing this image and checking if the registration, brain mask and midline are correct were the first steps in quality control. The values of the voxels can also be verified, but these values are different between patients. Generally, if the values were between the range of 20 and 100 ml/100 gr/min, the image was deemed acceptable. The average mean perfusion of grey matter given by the OXFORD_ASL tool was 29.8 with a standard deviation of 8.8. None of the patients we used in our research had artefacts, misregistrations or any other visual errors.

In the nifti folder are the graphs showing the translation and rotation done by the MCFLIRT tool. If these values are higher than 0.001 radian or lower than -0.001 for the rotation or higher than 1 millimetre or lower than 1 millimetre for the translation, the 4D files of the difference and tagged-untagged files should be checked to see if the registration was done correctly.

The registration of the DTI data is less sensitive to errors than the ASL data is. This results in a reduced number of errors in the output images, zero in our case. The FA values should be in the range of 0 to 1 and the MD values should have a maximum of 0.01, with most voxels having values in the range of 0 to 0.002. The edges of the brain and any rotation errors or artefacts should be easily distinguishable.

We tested the data by looking at Pearson's rho between the perfusion, FA and MD ratios in the same regions in the left and right hemisphere. All values correlate with p values under 0.001 between the left and right hemisphere. Therefore, we deemed our pipeline as functioning properly.

6 References

1. Woolrich, M. W. *et al.* Bayesian analysis of neuroimaging data in FSL. *Neuroimage* **45,** S173–86 (2009).
2. Smith, S. M. *et al.* Advances in functional and structural MR image analysis and implementation as FSL. *Neuroimage* **23 Suppl 1,** S208–19 (2004).
3. Jenkinson, M., Beckmann, C. F., Behrens, T. E. J., Woolrich, M. W. & Smith, S. M. FSL. *Neuroimage* **62,** 782–90 (2012).
4. Rorden, C. Rorden's DCM2NII. http://www.mccauslandcenter.sc.edu/mricro/mricron/ at <http://www.mccauslandcenter.sc.edu/mricro/mricron/dcm2nii.html>
5. Smith, S. M. Fast robust automated brain extraction. *Hum. Brain Mapp.* **17,** 143–155 (2002).
6. Jenkinson, M., Bannister, P., Brady, M. & Smith, S. Improved optimization for the robust and accurate linear registration and motion correction of brain images. *Neuroimage* **17,** 825–41 (2002).
7. Desikan, R. S. *et al.* An automated labeling system for subdividing the human cerebral cortex on MRI scans into gyral based regions of interest. *Neuroimage* **31,** 968–80 (2006).
8. Mori, S., Wakana, S., Lidia & van Zijl, P. MRI Atlas of Human White Matter. *AJNR Am. J. Neuroradiol.* **27,** 239 (2005).
9. Hua, K. *et al.* Tract probability maps in stereotaxic spaces: Analyses of white matter anatomy and tract-specific quantification. *Neuroimage* **39,** 336–347 (2008).
10. Jenkinson, M. & Smith, S. A global optimisation method for robust affine registration of brain images. *Med. Image Anal.* **5,** 143–56 (2001).
11. Chappell, M. A. *et al.* Partial volume correction of multiple inversion time arterial spin labeling MRI data. *Magn. Reson. Med.* **65,** 1173–83 (2011).
12. Chappell, M. A., Groves, A. R., Whitcher, B. & Woolrich, M. W. Variational Bayesian Inference for a Nonlinear Forward Model. *IEEE Trans. Signal Process.* **57,** 223–236 (2009).
13. Andersson, J. L. R. & Sotiropoulos, S. N. An integrated approach to correction for off-resonance effects and subject movement in diffusion MR imaging. *Neuroimage* **125,** 1063–1078 (2016).

Chapter 2

“Patient-Study”

7 Introduction

7.1 Alzheimer's Disease

The number of people currently living with Alzheimer's disease (AD) is estimated to 46.8 million people worldwide. This number is predicted to double every twenty years, resulting in 131.5 million people suffering from AD in 2050[14]. The worldwide cost of care for AD is around 818 billion United States dollars. This will increase to 1 trillion US dollars in 2018 and 2 trillion US dollars in 2030[14]. These costs are mostly made by the high income countries, with the G7 countries accounting for 92% of the costs.

Dementia is a spectrum of diseases all characterized by progressive deterioration of cognition, function and behaviour in patients. In the case of AD, symptoms include memory loss that disrupts daily life, time and place mismatches, difficulty in following instructions, difficulty in planning and solving problems, and problems with speech, writing and reading [15].

The mechanisms that cause AD are currently not fully understood despite a growing effort in the research community to discern their working. Research has found that amyloid plaques and neurofibrillary tangles (NFTs) are present in autopsied brains of patients with AD[16]. Amyloid plaques are seen in the extracellular matrix and in the walls of cerebral blood vessels. Accumulation of these plaques cause damage to the neurons and synapses. The amyloid plaques damage the mitochondria of cells and, therefore, causes an energy shortage and cell death [17–19]. NFTs consist of misfolded tau proteins and also is linked to mitochondrial oxidative stress [20,21].

The neurovascular homeostasis in patients with AD also receives more attention. The adaptability of the arteries and veins to variations in blood pressure by changing the vascular resistance plays an important role in supplying the brain with the materials for its energy consumption [22–24]. AD has many risk factors in common with vascular disease, such as Diabetes Mellitus, smoking and alcohol abuse, which may indicate that vascular damage is involved with AD [25]. The accumulation of NFTs and amyloid plaques can be explained by oxidative stress, which can also be caused by hypoperfusion. Evidence demonstrates that hypoperfusion of the brain precedes the clinical symptoms. This has led to an increase of research in the perfusion in the brain of patients with AD.

7.2 Brain Perfusion

Imaging techniques in the medical world have improved vastly in the last century. These improvements have given us new opportunities to study the brain and its perfusion. For AD, this includes structural magnetic resonance imaging (MRI), functional MRI methods, such as BOLD, ASL and DTI, Positron emission tomography (PET) and single photon emission computed tomography (SPECT). Ever since the invention of MRI 40 years ago, the MRI technique has been under constant development. Currently, it is the tool of choice for neuroimaging. It provides a strong grey and white matter contrast and can be adapted to acquire numerous types of biomarkers[26,27]. Since AD has been suspected of being a vascular disease, arterial spin labelling (ASL) gives a great opportunity to investigate the perfusion further. ASL perfusion scans have shown their merit in diagnosing acute stoke, chronic cerebrovascular diseases, tumour grades and the response to anti-angiogenesis therapy[28–30]. Patients with AD have decreased cerebral blood flow (CBF) in the precuneus, lateral parietal, inferior parietal, posterior cingulate and lateral prefrontal cortices and the hippocampus, making these areas of interest for further investigations[31–33].

In ASL sequences, blood is labelled by inverting the protons in blood just outside of the imaging plane. By using the flow of the blood, the magnetized protons arrive in local tissue. The labelled molecules can leave the capillary bed and, therefore, also be present in tissue other than arteries and

veins. The image is made after a set time, the post labelling delay (PLD), in which the blood can reach the parenchyma [34]. The acquired images are subtracted by a control image, acquired by the same protocol but without labelling of the blood as can be seen in Figure 2. The cerebral blood flow (CBF) in each voxel can then be calculated by using the following equation

$$CBF = \frac{6000 \times \lambda \times \Delta SI \times e^{\frac{PLD}{T_{1,blood}}}}{2 \times \alpha \times TI_{1,blood} \times SI_{PD} \times x_{new}} \qquad (2)$$

where λ is the brain/blood partition coefficient in mL/g, ΔSI is the difference in signal intensities between the control and label images, PLD is the pulse label duration, $T_{1,blood}$ is the longitudinal relaxation time of blood in seconds. SI_{PD} is the signal intensity of a proton density-weighted image, α is the labelling efficiency and x_{new} is the value of the voxel in the calibration image as calculated in equation 1 in chapter 1.

With this method, three assumptions are made:

1. The labelled blood arrives in its entirety in the target tissue.
2. No labelled blood flows out of the area.
3. The relaxation of the spins in the labelled blood is only dependant on the blood T_1.

The signal difference between labelled and unlabelled images are usually only one or two percent, leaving the inherent image with a low signal to noise ratio[35,36]. To improve this ratio, multiple images are acquired with different TIs. However, this makes this method susceptible to motion artefacts and makes background suppression a necessity. Post-processing can also enhance the images[37].

7.3 White Matter Integrity

To investigate the effect of disturbed perfusion on the brain, we have looked at the integrity of the white matter. To obtain a quantification of the integrity, we have used diffusion tensor imaging (DTI). DT images are created by using a diffusion contrast made available by MRI. DTI measures the mobility of water molecules. Water molecules are able to diffuse quicker in the length of axons in the white matter than in the width of the axons. By altering the direction in which we measure the mobility of the water molecules, a three dimensional vector of diffusion in each voxel can be made[38–41]. By using this vector, eigenvalues and eigenvectors can be calculated. These factors show direction and diffusivities along the primary axes of each voxel. This can be further explained by imagining the diffusion values of a voxel as an ellipsoid. The eigenvalue gives us the radii of the ellipsoid and eigenvectors give us the direction of the principal axes of this ellipsoid[38]. The eigenvalues can then be used to create different type of DT images. For a summary evaluation, fractional anisotropy (FA) can be calculated from the eigenvalues[42] by the following equation:

$$\mathrm{FA} = \frac{\sqrt{1}}{\sqrt{2}} \frac{\sqrt{(\lambda_1 - \lambda)^2 + (\lambda_2 - \lambda)^2 + (\lambda_3 - \lambda)^2}}{\sqrt{\lambda_1^2 + \lambda_2^2 + \lambda_3^2}} \qquad (3)$$

where λ is the average eigenvalue and λ_1, λ_2 and λ_3 are the magnitude of the eigenvalue per axis.

So FA gives us the relative difference between the largest vector, or eigenvalue, compared to the other two. It is highly sensitive in multiple brain pathologies, but gives no actual information about the shape of the ellipsoid or the type of damage occurring.

Mean diffusivity is calculated by averaging the three eigenvalues. This gives a quantification for membrane density, making it sensitive to oedema and necrosis.

The most common sequence for creating diffusion weighted images is by using a pulsed-gradient, spin echo with a single-shot, echo planar imaging (EPI) readout[42]. By dephasing and then rephrasing the molecules, stationary molecules will be cancelled out and only diffusing molecules will be imaged, also shown in figure 3.

7.4 Research Outline

Although the understanding of AD has increased over the last decades, there is still a large part of the disease that is not understood. It is unclear what causes the amyloid accumulation and its effect on the brain tissues is only partly understood. One of the hypothesized effects of amyloid plaques is that it harms the integrity of blood vessels. This is supported by the knowledge on the known decrease in cerebral perfusion in AD. However, there is currently a lack in understanding how different brain regions are affected, e.g. is the blood flow to the brain regions that are damaged in AD similarly influenced. The objective of this study was to gain understanding in the effects of AD on cerebral perfusion. The following research question was used:

"Is the perfusion of areas affected by Alzheimer's disease correlated?"

Literature reports a number of regions that show hypoperfusion in early AD. These areas are located in the posterior part of the brain. Our hypothesis was that the perfusion values of the areas affected by AD in the posterior part of the brain correlate with each other. The second hypothesis is that the perfusion values of the affected areas do not correlate with the perfusion values of a control area in the anterior part of the brain. Lastly, we expected that perfusion values of the affected areas would not correlate with an unaffected area in the posterior part of the brain.

In AD, the white matter tracts of the brain are affected as well. It is not currently known how this damage occurs. For instance, reduced perfusion in brain regions could cause damage to white matter tracts working with those regions. We wanted to investigate the effect of changed perfusion in certain areas on the integrity of the white matter tracts connecting those area to other areas. For this investigation, we already have selected areas affected by AD. These areas are generally connected by the cingulum. The cingulum, therefore, seems a good choice for use as a white matter tract. We used the following research question:

"Does the perfusion of brain regions affected by AD correlate with the white matter integrity of the cingulum?"

We suspected that when hypoperfusion occurs in cells, these cells die, causing the white matter integrity to decrease as well.

8 Methods

8.1 Subjects

In an ongoing trial, MR scans were made of 36 patients with mild to moderate AD. The main inclusion criteria were a diagnosis of probable AD, an age of over 50, a Mini-Mental State Exam (MMSE) of over 12 and under 27. Exclusion criteria were comorbidity in regards to dementia, structural abnormalities in the brain, patients with alcohol or drugs abuse and abnormal ECG results. Blood pressure values of under 100/65 mmHg or greater than 159/99 mmHg were also exclusion criteria. This was done because the intervention drug had an effect on blood pressure so the blood pressure was not allowed to be too low and by high values the drug would have a definite effect and that would result in the patients being unblinded.

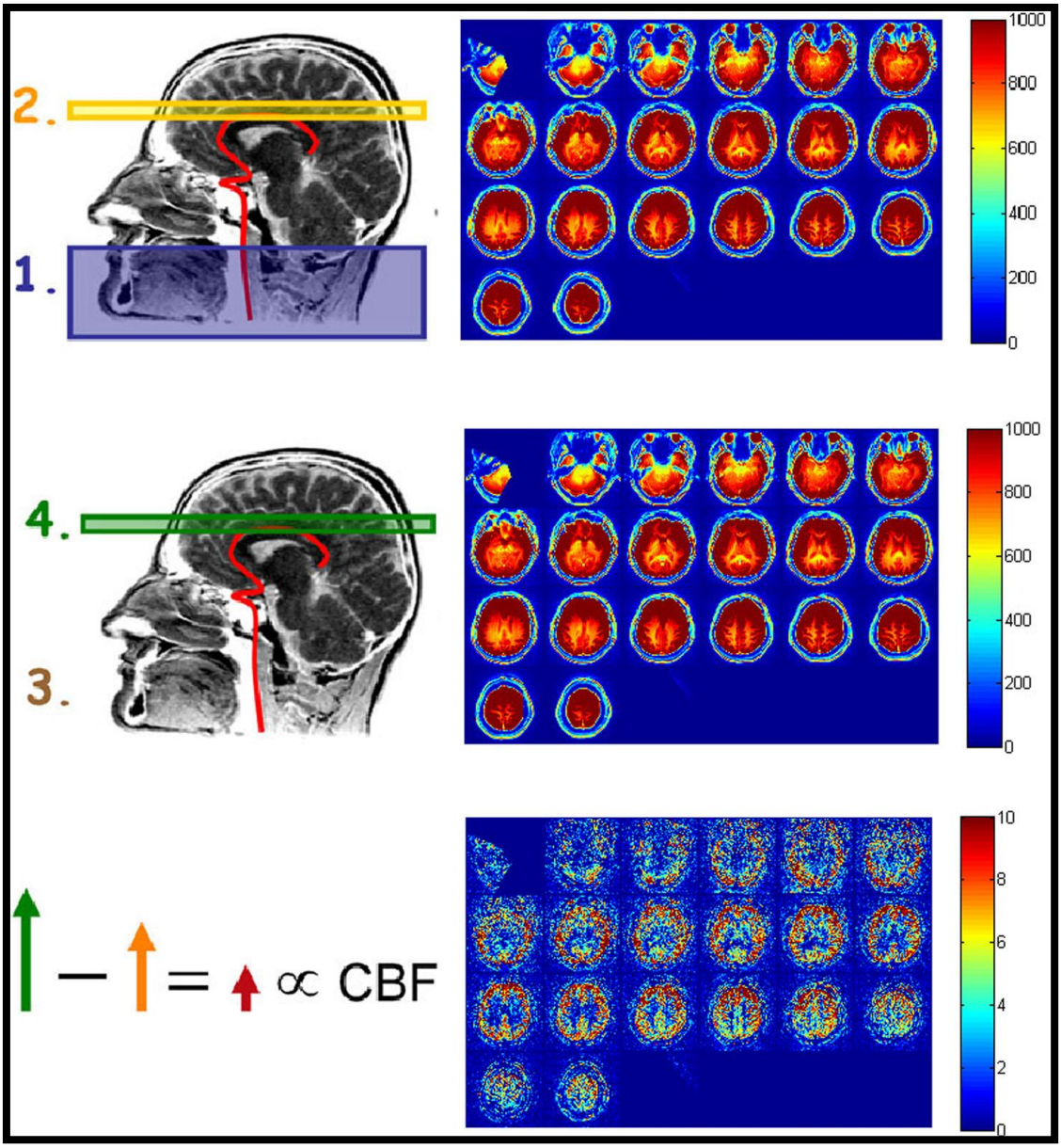

Figure 2: Principles of the ASL sequence and sample images. Blood gets tagged in slab 1 and measured in slab 2 of the tagged image. Then, a control image is made by imaging in the same slab (slab 4) without tagging the blood. By subtracting the control image from the tagged image, a difference map is created. ATT would be the time that the blood needs to travel from the labelling slab to the imaging slab. The colour bar represent the value of perfusion.

8.2 Data Acquisition

All patients underwent a MRI protocol which takes around an hour to complete. A 3-Tesla Siemens Magnetom TrioTim syngo machine was used. The pulsed ASL sequence is adapted for use in the elderly by using an adaptable post labelling delay. The delay starts at 500 milliseconds and each iteration adds 250 milliseconds. This allowed us to find the best delay, since the transit time of the blood will vary more in the brain of the elderly between subjects than in other age groups. The ASL sequence has the following parameters: a resolution of 3.4 by 3.4 by 4.0 millimetres, a FOV of 220 by 220 millimetres, a slice thickness of 4.0 millimetres, TE/TR 13.26/4000 milliseconds, a flip angle of 100 degrees, turbo/EPI factor of 23/12 and a bolus duration of 1400 milliseconds. 10 label and control images are acquired. Background suppression was used with pulses after 700 milliseconds

and 100 milliseconds into every iteration. A M0 quantification image with multiple timepoints was also created for calibration of the data.

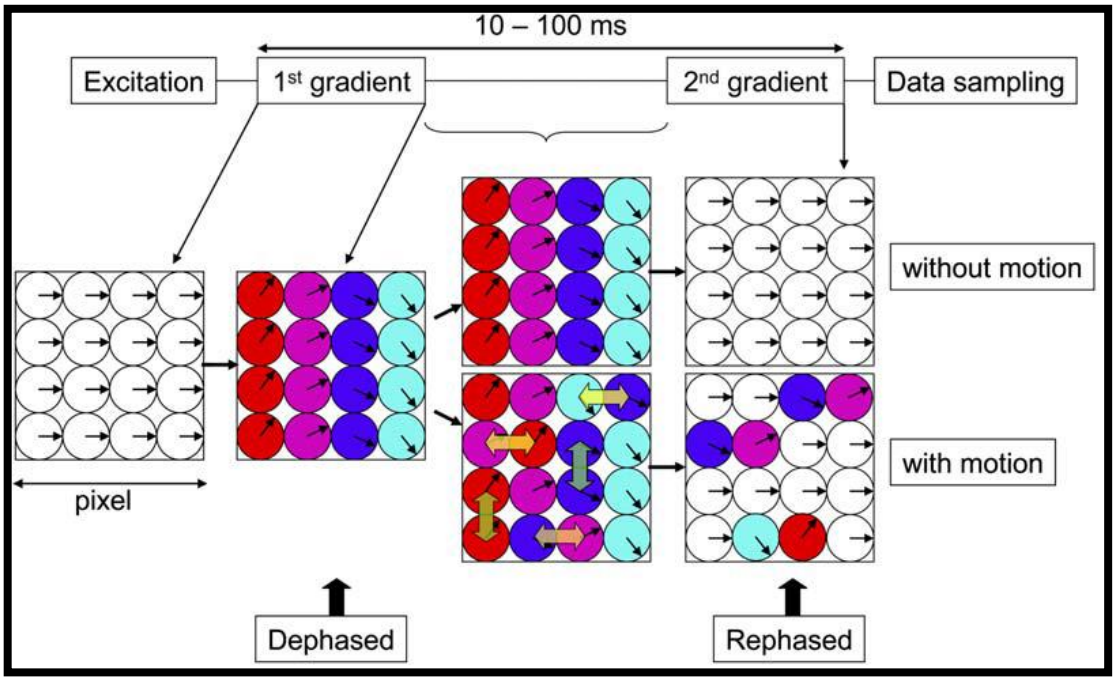

Figure 3: An illustration of the motion of water and its effect on magnetization. The circles represent the water molecules and the arrows their phase rotation. If they move between gradients, signal loss will occur because the gradient cannot totally refocus them. Courtesy of Mori et al[38].

The DTI sequence has the following parameters: a resolution of 2.0 by 2.0 by 2.0 millimetres, a FOV of 240 by 240 millimetres, a slice thickness of 2.0 millimetres, TE/TR 85/7400 milliseconds, a rotation angle of -0.20 degrees and EPI factor of 120. 64 diffusion directions are used and the b-value is 1000 s/mm^2.

8.3 *Post-Processing*

A script was created for automated sorting and post-processing of the ASL and DTI data. The script was created in Matlab R2015b using commands and functions of the FMRIB Software Library (FSL). A mask of the brain is created to filter the skull out of the ASL and DTI data. All ASL control and label data are then linearly registered to each other. This allowed for two transform matrices to be used for conversion to the brain mask and the MNI standard space. We created these transform matrices by linearly aligning the variance image created by MCFLIRT to the brain mask and the brain mask to the MNI space. Difference images for the ASL data are created by subtracting the control image from the labelled image. This creates perfusion maps that were further processed by the OXFORD_ASL toolbox to a single perfusion image. An example is shown in figure 4.

For the DT images, we first corrected for eddy currents. Next, we fitted a diffusion tensor model to each voxel. With these diffusion tensors, we created the FA and MD images. These images were also registered to the MNI standard brain and space so that they matched the space of the ASL data.

8.4 *Quality Control*

We checked every perfusion and DT image for artefacts and errors in registration. This was done by verifying if the contours of the brain were in the right place and if the space between the hemispheres was in the middle of the image as can be seen in figure 3 by the straight vertical line in the anterior part of the brain. We also checked if the average values of the perfusion of the grey and white matter that was given as an output by the OXFORD_ASL tool were between 20 and 50

ml/100gr/min. We used the atlas we created to ensure that the registration to the MNI standard space was done correctly.

8.5 *Analysis*

We selected a number of regions to investigate in this study. We selected regions affected by AD and a control region unaffected by AD, in this case the precentral gyrus. Most of the regions are in the posterior part of the brain, so we also selected a region in the posterior part, the occipital lobe, and one in the anterior part, the frontal lobe, as control regions and for investigating the effect of position in the brain on perfusion. We acquired these regions from the Harvard-Oxford Cortical and Subcortical Structural Atlas. We choose larger areas to compensate for the possible mismatches in registration between patients. For the white matter, we selected the cingulum, as this collection of tracts seemed to connect the selected regions. We extracted this tract from the JHU White-Matter Tractography Atlas. We created masks of these regions and calculated the mean voxel value of each region per patient.

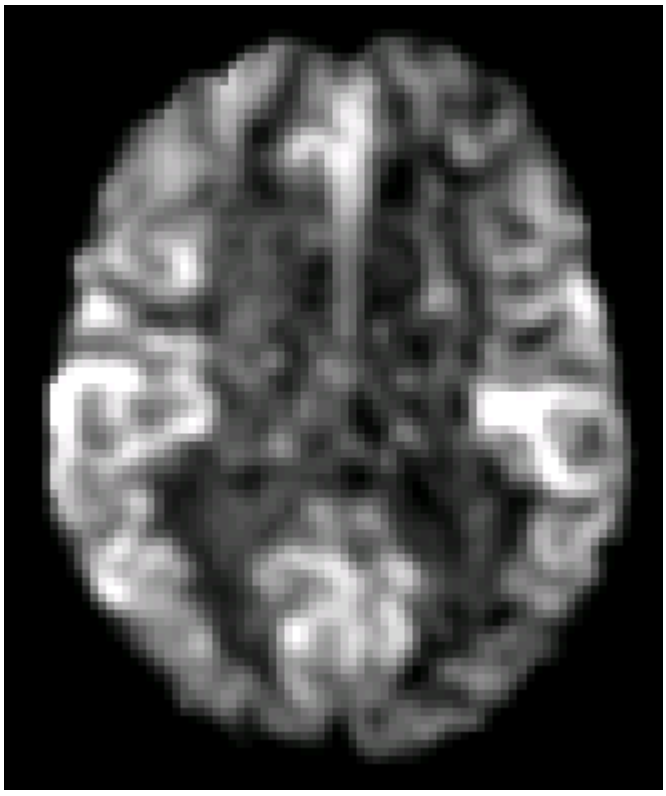

Figure 4: Perfusion image created by the OXFORD_ASL command. High perfusion voxels are shown in white and lower perfusion voxels in black.

Every human has different perfusion values. Therefore, we had to create a way to normalize the data. We did this by averaging the mean value of our control region of both the left and right hemisphere. We divided each mean perfusion value by this number to acquire data we could compare between patients. To be able to compare perfusion and the FA and MD values, we had to create the same ratios, so we normalized the FA and MD regions the same way.

All values were inserted in SPSS v. 22. We used SPSS to calculate Pearson's correlation of the perfusion in the different regions. Because of the large number of tests we do, we only consider p-values of under 0.01 to be significant and only consider regions where we see correlations in both the left and the right hemisphere to be relevant.

9 Results

Thirty-six datasets were acquired from patients with AD. The average age was 76±5 years. Twenty-five males and eleven females were included. MMSE scores had a mean of 20.6±3.2 points. The mean perfusion in the white matter was 24.4±7.3 ml/100gr/min and in grey matter 29.8±8.8 ml/100gr/min as given by the OXFORD_ASL tool.

To answer our research question, we want to determine the correlation between the perfusion of the selected regions and the FA and MD values of the connecting white matter tracts. We also checked for correlations between the regions affected by AD.

We show the correlations of the perfusion values of the regions affected by AD in table 2. The perfusion of the thalamus correlates with the hippocampus and the posterior cingulate gyrus in both hemispheres. The correlation between the posterior cingulate gyrus and the thalamus is very strong. There is also a correlation between the thalamus and the precuneus in the right hemisphere, but we do not see the same correlation in the left hemisphere so we see it as not significant. The perfusion of the hippocampus correlates with the anterior cingulate gyrus in both hemispheres next to the aforementioned thalamus. If we look at the superior parietal gyrus, we see that the perfusion values correlate with the perfusion values of the anterior cingulate gyrus and the precuneus in both hemispheres. The correlation between the anterior cingulate gyrus and the superior parietal is negative. The posterior cingulate gyrus correlates with the precuneus and the thalamus in both hemispheres, whereas the anterior part of the cingulate correlates with the hippocampus and the superior parietal gyrus. Lastly, the precuneus correlates with the superior parietal and the posterior cingulate gyri in both hemispheres.

Table 2: In this table, we show the Pearson's correlation and corresponding p-value between perfusion values of the regions. The correlations between areas in the left hemisphere can be seen above the black line and those of the right hemisphere can be seen under

Perfusion:	**Thalamus**	**Hippocampus**	**Superior Parietal Gyrus**	**Posterior Cingulate Gyrus**	**Anterior Cingulate Gyrus**	**Precuneus**
Thalamus	Left side →	0.437 (0.008)*	0.080 (0.641)	0.652 (<0.001)*	0.295 (0.081)	0.367 (0.028)
Hippocampus	0.506 (0.002)*	← Right side ↓	-0.282 (0.095)	0.388 (0.019)	0.659 (<0.001)*	-0.013 (0.941)
Superior Parietal Gyrus	0.315 (0.061)	-0.173 (0.314)		0.0069 (0.959)	-0.602 (<0.001)*	0.596 (<0.001)*
Posterior Cingulate Gyrus	0.597 (<0.001)*	0.325 (0.053)	0.171 (0.318)		0.285 (0.092)	0.471 (0.004)*
Anterior Cingulate Gyrus	0.094 (0.584)	0.546 (0.001)*	-0.569 (<0.001)*	0.219 (0.200)		-0.259 (0.126)
Precuneus	0.436 (0.008)*	-0.153 (0.373)	0.442 (0.007)*	0.439 (0.007)*	-0.361 (0.031)	

Table 3 shows the correlations of the control regions that we use. No significant correlations are seen in both hemispheres between the frontal lobe and the other regions. The occipital lobe's perfusion shows correlations with the superior part of the parietal gyrus and precuneus in both hemispheres.

Table 3: The Pearson's correlation and p-values of the investigated areas and the control regions are shown in this table. Note the values of the superior part of the Parietal gyrus and the Precuneus. Significant correlations are marked with an asterisk.

Perfusion: *Left Side*	**Thalamus**	**Hippocampus**	**Superior Parietal Gyrus**	**Posterior Cingulate Gyrus**	**Anterior Cingulate Gyrus**	**Precuneus**
Frontal Lobe	0.076 (0.658)	0.241 (0.158)	-0.064 (0.710)	0.348 (0.037)	0.095 (0.583)	-0.049 (0.777)
Occipital Lobe	0.364 (0.029)	-0.056 (0.746)	0.634 (<0.001)*	0.413 (0.012)	-0.278 (0.101)	0.520 (0.001)*
Right Side						
Frontal Lobe	0.185 (0.279)	0.042 (0.810)	0.230 (0.178)	0.427 (0.009)*	-0.014 (0.936)	0.149 (0.385)
Occipital Lobe	0.505 (0.002)*	0.145 (0.397)	0.593 (<0.001)*	0.571 (<0.001)*	-0.328 (0.051)	0.483 (0.003)*

Table 4: The Pearson's correlation and p-values of the regions affected by AD and the FA and MD values of the posterior part of the cingulum.

Perfusion: *Left side*	**Thalamus**	**Hippocampus**	**Superior Parietal Gyrus**	**Posterior Cingulate Gyrus**	**Anterior Cingulate Gyrus**	**Precuneus**
FA cingulum Posterior	-0.034 (0.844)	0.014 (0.945)	-0.325 (0.053)	-0.041 (0.811)	0.156 (0.362)	-0.191 (0.264)
MD cingulum Posterior	-0.190 (0.266)	0.071 (0.680)	0.088 (0.610)	-0.177 (0.301)	-0.099 (0.567)	0.300 (0.075)
Right side						
FA cingulum Posterior	-0.295 (0.081)	-0.149 (0.385)	-0.300 (0.076)	-0.327 (0.051)	0.032 (0.853)	-0.373 (0.025)
MD cingulum Posterior	-0.132 (0.443)	-0.138 (0.422)	-0.064 (0.712)	-0.037 (0.832)	-0.049 (0.775)	0.385 (0.020)

Tables 4 and 5 show the correlations between the white matter integrity, in the form of FA and MD, and the perfusion of the areas we investigated. The FA and MD values of the posterior cingulum shown no correlations as can be seen in table 4. Most correlations in the table do show a negative correlation, but these are not significant. Table 5 shows that the thalamus and the FA values of the anterior cingulum have a negative correlation. The rest of the values show no significant correlations but most have negative values similar to table 4.

Table 5: The Pearson's correlation and p-values of the regions affected by AD and the FA and MD values of the anterior part of the cingulum. Of note are the values of the Thalamus and the FA of the cingulum. Significant correlations are marked with an asterisk.

Perfusion: *Left side*	**Thalamus**	**Hippocampus**	**Superior Parietal**	**Posterior Cingulate gyrus**	**Anterior Cingulate gyrus**	**Precuneus**
FA cingulum Anterior	-0.428 (0.009)*	0.274 (0.106)	-0.291 (0.085)	-0.402 (0.015)	-0.007 (0.968)	-0.119 (0.490)
MD cingulum Anterior	-0.072 (0.675)	-0.231 (0.176)	0.180 (0.294)	-0.185 (0.281)	-0.271 (0.110)	0.301 (0.074)
Right side						
FA cingulum Anterior	-0.510 (0.001)*	-0.305 (0.071)	-0.284 (0.094)	-0.316 (0.060)	0.039 (0.823)	-0.003 (0.986)
MD cingulum Anterior	-0.065 (0.706)	-0.272 (0.108)	-0.014 (0.934)	-0.348 (0.038)	-0.244 (0.151)	0.247 (0.147)

10 Discussion

In this study, we have used a novel arterial spin labelling sequence to investigate the link between the perfusion of areas affected by AD. We combined ASL and DT images to investigate the effect of perfusion on the white matter integrity. The data did not support a link between perfusion and white matter integrity.

We found a number of areas of which the perfusion correlates. We do not see correlations in all areas, but in enough areas to think this is a significant discovery. Multiple studies with ASL and AD show the areas we used as ROIs have reduced perfusion in patients with AD[43–47]. Our results show that the perfusion values of these areas are linked. We see connected perfusion between the hippocampus, thalamus and posterior part of the cingulum. We do not see connections if we compare the perfusion values of these regions with the frontal lobe, which is not affected in the early stages of AD. If we compare the values of our AD ROIs with an area in the posterior part of the brain unaffected in the early stages of AD, the occipital lobe, we do see correlations. This might indicate that the location of the ROIs has an influence on the found correlations. Most of our AD regions are supplied by the posterior cerebral artery or one of its branches. Perfusion is an indication of blood flow to a region and lower perfusion values are likely indicators of reduced flow. Reduced flow can be an indication of reduced ability of vessels to supply blood to a region. Therefore, we think that perfusion as measured by ASL could be an indicator for the status of a blood vessel. Perfusion, however, does not tell us anything as to why the vessels are impaired. Although we cannot say if the entire posterior cerebral artery is affected, it does seem that the integrity of this vessel and its branches is somehow impaired. This would be an interesting subject for future research.

Our results show no correlation between the perfusion of the ROIs and the white matter integrity, in the form of the FA and MD values, of the cingulum. The only exception is the thalamus. In this area we see a negative correlation between perfusion and the FA values. In the rest of the areas we also negative correlations, but none are significant. Assuming our methods are correct, the negative correlation is an interesting effect. It indicates that if the integrity of the white matter tracts decreases, the perfusion values are higher and vice versa. Although we do not have the data to give an informed explanation for these findings, we do have a number of theories. It is possible the brain

region compensates for the damage to the white matter by becoming more active and, therefore, need more blood to function. It could be possible that when the connections between regions degrade, to maintain efficient communication, the brain regions need to create more signals or passes its functions to areas within the same region, which causes more cells to become active. This would result in a higher blood flow. This would explain why the CBF gets higher when the white matter integrity becomes lower.

Another possible explanation might be that there is a form of inflammatory response around the white matter that causes additional blood flow the surrounding area. There has been some evidence that neuroinflammation is seen in the development of AD[48–50]. Neuroinflammation may be caused by infections or toxic metabolites. Toxic metabolites in this case could be the amyloid-β deposits seen in AD.

10.1 Methodical Strengths and Weaknesses

We have shown that data corresponding with past research can be acquired by using an ASL sequence that has multiple inversion times for correction of differences in arrival time of blood in elderly patients.

A limitation of this study is that we do not have a healthy control group to compare our data to. This means that all of our findings could be seen in a healthy population. Although our results might differ in healthy controls, the correlations seen remain interesting. There is the possibility that our findings are already affected by AD and that in a healthy control group, more correlations in perfusion could be found.

ASL creates images of low resolution and a high signal-to-noise ratio. This makes it difficult to register the images to a standard space. This can create mismatches between the images and the regions that we use. This could distort our data. Although we checked every image on large mismatches, mismatches of a few voxels could be overlooked. We compensated this effect by using large areas. The few mismatching voxels around the edges should be of insignificant number compared to the total number of voxels and, therefore, not or barely influence our results.

The low resolution makes it difficult to determine the edges of the brain. By using a mask created from the T1 weighted image, we guessed the edges, but it could be that we cut of parts of the edges. There is currently no way of knowing whether or not we did this, but it is a possibility. If this occurs, it is possible this is corrected by the automation of our pipeline. The error should at least be a systematic error. The number of voxels cut would be small in comparison with the entire regions. This would prevent it from changing the interpatient results.

We also used the normalization for our FA values. In hindsight, FA values should be comparable between patients without this normalization, so this would not have been necessary. We do not think this caused any errors in our data, but it should be mentioned.

In conclusion, we have shown that the perfusion of regions in the posterior part of the brain in AD correlates. Our results do not support the existence of any correlations between perfusion and white matter integrity.

11 References

14. Prince, M. *et al. World Alzheimer Report 2015: The Global Impact of Dementia - An analysis of prevalence, incidence, cost And trends*. (2015). doi:10.1111/j.0963-7214.2004.00293.x

15. Association, A. 2013 Alzheimer's disease facts and figures. *Alzheimer's Dement.* **9,** 208–245

(2013).

16. Kumar, A. & Singh, A. A review on Alzheimer's disease pathophysiology and its management: an update. *Pharmacol. Reports* **67,** 195–203 (2015).

17. Simoncini, C. *et al.* Alzheimer's Pathogenesis and Its Link to the Mitochondrion. *Oxid. Med. Cell. Longev.* **2015,** 1–8 (2015).

18. Wang, X. *et al.* The role of abnormal mitochondrial dynamics in the pathogenesis of Alzheimer's disease. *J. Neurochem.* **109,** 153–159 (2009).

19. Zhu, X., Perry, G., Smith, M. a & Wang, X. Abnormal mitochondrial dynamics in the pathogenesis of Alzheimer's disease. *J. Alzheimers. Dis.* **33 Suppl 1,** S253–62 (2013).

20. Melov, S. *et al.* Mitochondrial oxidative stress causes hyperphosphorylation of tau. *PLoS One* **2,** e536 (2007).

21. Lin, M. T. & Beal, M. F. Mitochondrial dysfunction and oxidative stress in neurodegenerative diseases. *Nature* **443,** 787–95 (2006).

22. Canobbio, I., Abubaker, A. A., Visconte, C., Torti, M. & Pula, G. Role of amyloid peptides in vascular dysfunction and platelet dysregulation in Alzheimer's disease. *Front. Cell. Neurosci.* **9,** 1–15 (2015).

23. Querfurth, H. W. & Laferla, F. M. Alzheimer's Disease. *N. Engl. J. Med.* **362,** 329–344 (2010).

24. Di Marco, L. Y., Farkas, E., Martin, C., Venneri, A. & Frangi, A. F. Is Vasomotion in Cerebral Arteries Impaired in Alzheimer's Disease? *J. Alzheimer's Dis.* **46,** 35–53 (2015).

25. de la Torre, J. C. Alzheimer disease as a Vascular Disorder: Nosological Evidence. *Stroke.* 1152–1162 (2002).

26. Jack, C. & Knopman, D. Update on hypothetical model of Alzheimer's disease biomarkers. *Lancet …* **12,** 207–216 (2013).

27. McKhann, G. M. *et al.* The diagnosis of dementia due to Alzheimer's disease: Recommendations from the National Institute on Aging-Alzheimer's Association workgroups on diagnostic guidelines for Alzheimer's disease. *Alzheimer's and Dementia* **7,** 263–269 (2011).

28. Zou, J.-X., Wang, M.-J., Lei, X.-J. & Chen, X.-G. 3.0T MRI arterial spin labeling and magnetic resonance spectroscopy technology in the application of Alzheimer's disease. *Exp. Gerontol.* **60,** 31–36 (2014).

29. Alsop, D. C., Dai, W., Grossman, M. & Detre, J. A. Arterial spin labeling blood flow MRI: Its Role in the early characterization of Alzheimer's disease. *Journal of Alzheimer's Disease* (2010). doi:10.3233/JAD-2010-091699

30. Dai, W. *et al.* Mild Cognitive Impairment and Alzheimer Disease: Patterns of Altered Cerebral Blood Flow at MR Imaging1. *Radiology* **250,** 856–866 (2009).

31. Sperling, R. A. *et al.* Toward defining the preclinical stages of Alzheimer's disease: Recommendations from the National Institute on Aging-Alzheimer's Association workgroups on diagnostic guidelines for Alzheimer's disease Reisa. *Alzheimer's Dement.* **7,** 280–292 (2011).

32. Viallon, M. *et al.* State-of-the-art MRI techniques in neuroradiology: principles, pitfalls, and clinical applications. *Neuroradiology* 441–467 (2015). doi:10.1007/s00234-015-1500-1

33. Yoshiura, T. *et al.* Arterial spin labelling at 3-T MR imaging for detection of individuals with

Alzheimer's disease. *Eur. Radiol.* **19,** 2819–2825 (2009).

34. Yang, Y. Perfusion MR imaging with pulsed arterial spin-labeling: Basic principles and applications in functional brain imaging. *Concepts Magn. Reson.* **14,** 347–357 (2002).

35. Pollock, J. M. *et al.* Arterial Spin Labeled MRI Perfusion Imaging: Clinical Applications. *Magn Reson Imaging Clin N Am* **17,** 315–338 (2009).

36. Jahng, G.-H. *et al.* Human brain: reliability and reproducibility of pulsed arterial spin-labeling perfusion MR imaging. *Radiology* **234,** 909–916 (2005).

37. Deibler, a. R. *et al.* Arterial spin-labeling in routine clinical practice, part 1: Technique and artifacts. *Am. J. Neuroradiol.* **29,** 1228–1234 (2008).

38. Mori, S. & Zhang, J. Principles of diffusion tensor imaging and its applications to basic neuroscience research. *Neuron* **51,** 527–39 (2006).

39. Hüppi, P. S. & Dubois, J. Diffusion tensor imaging of brain development. *Semin. Fetal Neonatal Med.* **11,** 489–97 (2006).

40. Farzinfar, M. *et al.* Diffusion imaging quality control via entropy of principal direction distribution. *Neuroimage* **82,** 1–12 (2013).

41. Alexander, A. L., Lee, J. E., Lazar, M. & Field, A. S. Diffusion tensor imaging of the brain. *Neurotherapeutics* **4,** 316–29 (2007).

42. Alexander, A. L., Lee, J. E., Lazar, M. & Field, A. S. Diffusion tensor imaging of the brain. *Neurotherapeutics* **4,** 316–29 (2007).

43. Verfaillie, S. C. J. *et al.* Cerebral perfusion and glucose metabolism in Alzheimer's disease and frontotemporal dementia: two sides of the same coin? *Eur. Radiol.* (2015). doi:10.1007/s00330-015-3696-1

44. Wolk, D. a. & Detre, J. a. Arterial spin labeling MRI: An emerging biomarker for Alzheimer's disease and other neurodegenerative conditions. *Curr. Opin. Neurol.* **25,** 421–428 (2012).

45. Alsop, D. C., Dai, W., Grossman, M. & Detre, J. A. Arterial spin labeling blood flow MRI: Its Role in the early characterization of Alzheimer's disease. *Journal of Alzheimer's Disease* **20,** 871–880 (2010).

46. Ding, B. *et al.* Pattern of cerebral hyperperfusion in Alzheimer's disease and amnestic mild cognitive impairment using voxel-based analysis of 3D arterial spin-labeling imaging: Initial experience. *Clin. Interv. Aging* **9,** 493–500 (2014).

47. Binnewijzend, M. a. a. *et al.* Cerebral perfusion in the predementia stages of Alzheimer's disease. *Eur. Radiol.* (2015). doi:10.1007/s00330-015-3834-9

48. Janssen, B. *et al.* Imaging of Neuroinflammation in Alzheimer's Disease, Multiple Sclerosis and Stroke: Recent Developments in Positron Emission Tomography. *Biochim. Biophys. Acta* **1862,** 425–441 (2015).

49. Renard, D. *et al.* Cerebrospinal Fluid Alzheimer's Disease Biomarkers in Cerebral Amyloid Angiopathy-Related Inflammation. *J. Alzheimers. Dis.* **50,** 759–764 (2016).

50. Giannoni, P. *et al.* Cerebrovascular pathology during the progression of experimental Alzheimer's disease. *Neurobiol. Dis.* **88,** 107–17 (2016).

Chapter 3
“Recommendations”

12 Pipeline

The pipeline that we created has shown to work on our patient group without errors. The major improvement here should be in the registration of the ASL data to the standard space. Currently, the pipeline uses the same transformation matrix for both the tagged as the untagged images. We suggest that a transformation matrix is made for both separately.

The current pipeline has a number of variables that have to be changed if the sequences are changed. For instance, the names that are used for sorting the data would have to be changed, but also the TI values. This could be more automated by using the UIGETFILE command that we use, although this must be used for each different file type. If all the names of the images are different, it is going to be difficult and another solution would have to be found. It might be useful to build a GUI so you can enter all variables that are needed and you can do QC while running the program.

A consideration would be to use the T1 image for the creation and selection of the regions of interest. Currently, we use the same regions for each patient, thus these regions are not selective per patient. Usually, the edges of the regions fall outside of the brain. We could create the regions for each patient individually by using the T1 image. This way, we can get a better grey matter only region. Although we believe the translation of most perfusion images to be correct, this could make the process more precise. However, since there is no way to verify the correct registration, taking smaller regions could induce larger errors. We would use very thin regions for the grey matter only. If the registration is of by a few voxels, this would be a greater problem if the regions are smaller, since the number of wrong voxels would be higher in the terms of percentage, as in this case, than when we use larger regions.

13 Future Research

First, we would compare this data with the data acquired during the other two measurement points. This could show changes in perfusion and white matter degradation. It should be noted that these patients al underwent intervention in the form of a potentially brain-perfusion stimulating drug or a placebo. It would be important to split the groups. It would be interesting to see what AD does to perfusion over time.

We recommend doing more research into the posterior cerebral artery (PCA) and its role in AD. By using MRA, the status of the PCA can be investigated in AD and healthy controls. Amyloid beta is usually seen in vessel walls. With magnetic resonance spectroscopy (MRS) or nuclear magnetic resonance spectroscopy (NMRS), the vessel walls could be imaged and its composition could be measured over time. This would give us further insight in the effect of the blood vessels on the brain tissue.

NMRS and MRS could be used to investigate the effect of inflammation on AD. The first step in this direction would be to compare our data to data acquired in healthy controls, to see if we indeed see hyperperfusion. If this is the case, further insight into neuroinflammation would be an interesting avenue to access.